Microhardness and heat-resistance performance of ferromagnetic cobalt-molybdenum nanocrystals electrodeposited from an aqueous solution containing citric acid

To cite this article: Tomoyuki Matsuda *et al* 2022 *Mater. Res. Express* **9** 046502

Materials Research Express

PAPER

Microhardness and heat-resistance performance of ferromagnetic cobalt-molybdenum nanocrystals electrodeposited from an aqueous solution containing citric acid

Tomoyuki Matsuda[1], **Ryusei Saeki**[1], **Masamitsu Hayashida**[2] **and Takeshi Ohgai**[2]

[1] Graduate School of Engineering, Nagasaki University, Bunkyo-machi 1-14, Nagasaki 852-8521, Japan
[2] Faculty of Engineering, Nagasaki University, Bunkyo-machi 1-14, Nagasaki 852-8521, Japan

E-mail: ohgai@nagasaki-u.ac.jp

Keywords: electrodeposition, cobalt, molybdenum, nanocrystal, microhardness, heat resistance

OPEN ACCESS

RECEIVED
9 January 2022

REVISED
16 March 2022

ACCEPTED FOR PUBLICATION
24 March 2022

PUBLISHED
6 April 2022

Abstract

Using a potentiostatic electrodeposition technique, nanocrystalline cobalt-molybdenum (Co-Mo) superalloys containing molybdenum oxide (MoO_X) were synthesized from an aqueous solution containing citric acid. Molybdenum content in the alloys was controlled up to approximately 53% by adjusting the cathode potential during the alloy electrodeposition. Based on the XRD profiles and electron diffraction patterns, an amorphous-like nanocrystalline structure was observed in the alloys with high molybdenum content. XPS analysis revealed that the chemical state of electrodeposited molybdenum was almost metallic and the oxide state was also detected partially. According to the magnetization curves, the coercivity of electrodeposited Co-Mo alloys decreased down to approximately 72 Oe with increasing the molybdenum content up to around 53%. The microhardness reached 845 kgf mm^{-2} in the electrodeposited Co-53%Mo alloy and greatly exceeded that of pure cobalt (ca. 250–300 kgf mm^{-2}). Heat resistance performance of the electrodeposited nanocrystalline Co-53%Mo alloy was improved by the Mo alloying effect because the recrystallization and oxidation behavior were not observed even if the annealing temperature was increased up to 700 °C.

1. Introduction

Hard chromium electroplating is one of the most widely used process in industrial metal surface finishing plants. The chromium electroplating technique has been used for the conventional mechanical parts that requires wear-resistant performance because of the significantly large hardness, excellent wear-resistance, and low friction coefficient [1, 2]. However, hexavalent chromium ions, which are contained in a hard chromium electroplating bath, are known as an extremely strong oxidizer. Therefore, its toxicity, such as causing inflammation of the skin and mucous membranes, is focused recently. In 2019, RoHS restricts to contain hexavalent chromium ions in all electronic devices in the EU. Hence, an alternative electroplating bath, which contains trivalent chromium ions, has been propose so far [3–6]. On the other hand, the electroplating of iron-group metals (Fe, Co, and Ni) and the alloys with an amorphous-like nanocrystalline structure is one of the alternative processes for the hard chromium electroplating [7, 8]. Because the amorphous-like nanocrystalline structure has an excellent hardness and corrosion resistance. It is well known that the corrosion resistance of bcc-Fe is not better than those of fcc-Ni and hcp-Co according to their standard electrode potential. On the contrary, the saturation magnetization of fcc-Ni is smaller than those of bcc-Fe and hcp-Co due to the number of lone-pair electrons which corresponds to the catalytic ability. Unlike the performance of bcc-Fe and fcc-Ni, the corrosion resistance and catalytic ability of hcp-Co are both excellent among the conventional metallic materials. Hence, the cobalt-based alloy coating technique can be an alternative candidate for the hard chromium electroplating process which utilize the toxic hexavalent chromium ions. As an additive element to the cobalt-based alloys, a metallic element with a high melting point will be effective to enhance the hardness and corrosion resistance. Especially, molybdenum has a quite high melting point (Mo: 2623 °C) rather than the iron-group metals (Fe: 1538 °C, Co: 1495 °C, and Ni:

1455 °C). It is well known that molybdenum is not able to be electrodeposited from an aqueous solution as a pure metallic state. However, even in an aqueous solution, molybdenum can be electrodeposited as a metallic alloy state with the iron-group metals. Brenner *et al* defined the alloys electrodeposition process as an '*induced co-deposition type*' [9]. The Co-Mo alloys, which are obtained by the '*induced co-deposition process*', exhibit the characteristic performance such as magnetism [10–14], corrosion-resistance [15–17], hydrogen evolution catalyst [18–23], and so on. Pellicer *et al* reported that Co-Mo alloys were electrodeposited by utilizing the reverse pulse plating method [24]. They revealed that the Vickers hardness of electrodeposited Co-38wt.%Mo alloys was 325 kgf mm^{-2} ($HV_{0.05}$). Krawiec *et al* also reported that Co-Mo/TiO_2 nano-composite films were electrodeposited from an aqueous solution containing TiO_2 nanoparticles [25]. They revealed that the Vickers hardness of electrodeposited Co-15at.%Mo/TiO_2 nano-composite films was around 700 kgf mm^{-2} (HV). Hardness of electrodeposited Co-Mo alloys should be enhanced with an increase in Mo content in the deposits. Hence, in the present study, Co-Mo alloys with Mo content more than 50at.% were synthesized by utilizing a potentiostatic electrodeposition technique with significant large overpotential [26] to achieve the Vickers hardness beyond 800 kgf mm^{-2} (HV). The nanocrystalline structure and heat resistance performance of the electrodeposited Co-Mo alloys were also investigated.

2. Method

An aqueous solution containing Co^{2+} and MoO_4^{2-} ions (Co-Mo mixture bath) was synthesized from 0.4 M cobalt sulfate heptahydrate, 0.1 M sodium molybdate dihydrate, 0.5 M sodium citrate dihydrate, 0.5 M boric acid. For comparison, an aqueous solution containing only Co^{2+} ions (pure Co bath) was also prepared from 0.4 M cobalt sulfate heptahydrate, 0.5 M sodium citrate dihydrate, 0.5 M boric acid. The solution temperature and pH were adjusted to 40 °C and 6.0, respectively, while the electrolytic bath was stirred using a magnetic stirrer (300 rpm) during the electrodeposition. A copper foil and a gold wire were utilized as a cathode and an anode, respectively, while a silver chloride electrode (Ag/AgCl/Sat. KCl) was used as a reference electrode. Cathodic polarization curves were investigated using an automatic polarization system (Electrochemical Measurement System, HZ-7000, Hokuto Denko Corp., Tokyo, Japan) to determine the optimum cathode potential range. Co–Mo alloys were synthesized by using a potentiostatic electrodeposition technique. Cathode potentials during the electrodeposition were fixed to the range from −1.2 V to −1.7 V versus Ag/AgCl. The alloy composition of electrodeposited Co–Mo alloys was determined using energy dispersive X-ray spectroscopy (EDX, EDX-800HS, Shimadzu Corp., Kyoto, Japan). Surface texture of the electrodeposited alloy samples was investigated using Scanning Electron Microscopy (SEM, JCM-5700, JEOL Ltd, Tokyo, Japan). Constituent phases were identified using Transmission Electron Microscopy (TEM, JEM-2010-HT, JEOL Ltd, Tokyo, Japan) and an X-Ray Diffractometer (XRD, Miniflex 600-DX, Rigaku Corp., Tokyo, Japan). Chemical state of molybdenum in the electrodeposited samples was analyzed using X-ray Photoelectron Spectroscopy (XPS, AXIS-ULTRA, Shimadzu Corp., Kyoto, Japan). Saturation magnetization of the electrodeposited films was investigated using a Vibrating Sample Magnetometer (VSM, TM-VSM1014-CRO, Tamakawa Co., Sendai, Japan) at room temperature. Microhardness of the electrodeposited films was measured using a micro-Vickers hardness testing machine (HM-211, Mitutoyo, Kanagawa, Japan). The microhardness test was performed on a polished cross-section of the electrodeposited films by applying a load of 0.1 kgf.

3. Results and discussion

3.1. Electrodeposition process of Co–Mo alloys

To compare the electrodeposition behavior of pure Co and Co–Mo alloys, each cathodic polarization curve was plotted as shown in figure 1(a). During the polarization measurement, the cathode potential was scanned at a rate of 50 mV s^{-1}. By scanning the potential to a less-noble region, the cathode current density began to increase sharply at approximately −0.8 V versus Ag/AgCl in both pure Co bath and Co-Mo mixture bath. According to Nernst's equation, the equilibrium potential of Co/Co^{2+} (E_{Co}^{eq}) can be calculated to approximately −0.49 V versus Ag/AgCl based on the bath temperature and metal ions concentration (40 °C, $[Co^{2+}] = 0.4$ M) [27]. Hence, the increase in the cathode current density should be caused by the deposition current of Co-Citrate complex ions as well as the reduction current of hydrogen ions [28, 29]. Subsequently, with an increase in cathode current density up to approximately 400 A m^{-2}, the cathode potential polarized to around −1.1 V versus Ag/AgCl in pure Co bath. On the contrary, in Co-Mo mixture bath, with increasing the cathode current density up to about 40 A m^{-2}, the cathode potential shifted to around −1.1 V and subsequently the cathode current density increased again up to approximately 200 A m^{-2}. This cathode potential shift at about 40 A m^{-2} seems to be caused by the adhesion of MoO_4^{2-} ions or molybdenum hydroxide [30, 31]. Hence, it is considered that the electrodeposition of Co-Mo alloy began to proceed at around −1.1 V due to the induced co-deposition

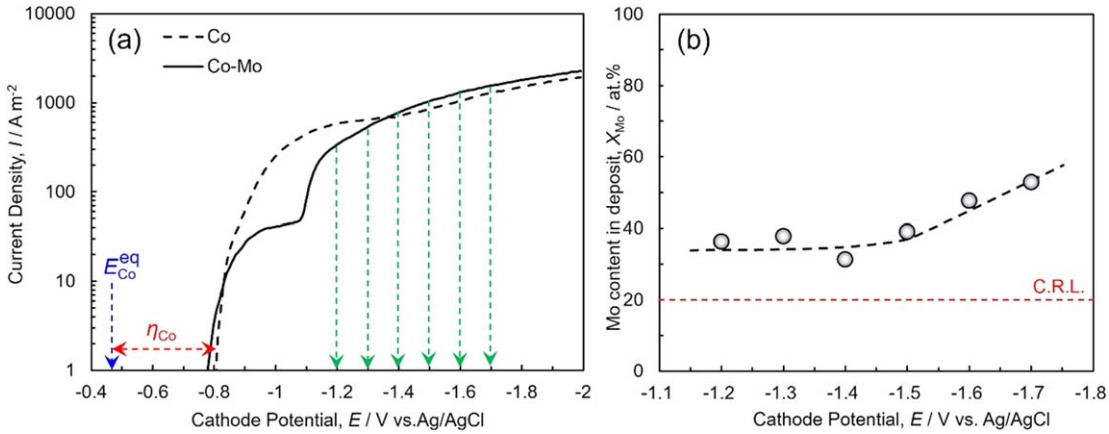

Figure 1. Cathodic polarization curve (Tafel plot) for electrodeposition of Co-Mo alloy from an aqueous solution containing citric acid (a). Effect of cathode potential on the molybdenum content (X_{Mo}) in electrodeposited Co-Mo alloys (b).

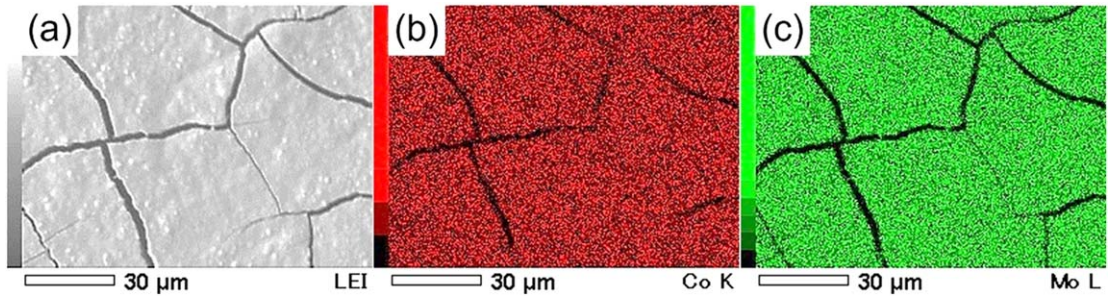

Figure 2. SEM image (a) of Co-36% Mo alloy electrodeposited at the cathode potential of −1.2 V versus Ag/AgCl. EDS elemental mapping images on cobalt (b) and molybdenum (c) in the electrodeposited alloy.

process [9]. Furthermore, with increasing the cathode current density more than about 1000 A m^{-2}, the slope of the polarization curve decreased and the cathode potential polarized significantly to a less noble region than −1.8 V versus Ag/AgCl in both pure Co bath and Co-Mo mixture bath. This significant polarization seems to be caused due to a decrease in the concentration of H^+, Co^{2+} and MoO_4^{2-} ions in the vicinity of cathode. Consequently, for electrodepositing Co-Mo alloys, the optimum cathode potential condition was determined, ranging from −1.2 V to −1.7 V versus Ag/AgCl.

Figure 1(b) shows the effect of cathode potential on the molybdenum content (X_{Mo}) in Co–Mo alloys. With shifting the cathode potential to a less-noble region, X_{Mo} in the alloys increased from approximately 36% to 53%. As shown in red dashed line in figure 1(b), the composition reference line (C.R.L.) is 20% which is identical to the ratio of MoO_4^{2-} ions concentration ([MoO_4^{2-}]) to the total metal ions concentration ([MoO_4^{2-}] + [Co^{2+}]). Hence, the molybdenum atoms in the alloy deposits seem to be condensed from the electrolytic bath due to the induced co-deposition process [32].

3.2. Surface appearance, constituent phase and chemical state of electrodeposited Co–Mo alloys

Figure 2 shows the SEM image (a) of Co-36% Mo alloy electrodeposited at the cathode potential of −1.2 V versus Ag/AgCl. The EDS elemental mapping images on cobalt (b) and molybdenum (c) are also shown in figures 2(b) and (c), respectively. The sample had some microcracks and small nodules as shown in figure 2(a). The elements for cobalt and molybdenum were homogeneously dispersed in the electrodeposited alloy as shown in figures 2(b) and (c). Hence, the electrodeposited Co-36% Mo alloy seems to be quite hard and brittle performance due to the formation of supersaturated solid solution phase.

Figure 3 shows the effect of cathode potential on the SEM images of Co–Mo alloys which were electrodeposited at the cathode potential range from −1.2 V to −1.7 V versus Ag/AgCl. All samples had some microcracks and nodules as shown in figure 3. Especially, numerous nodules were observed on the surface of the samples which were electrodeposited at the cathode potential range from −1.5 V to −1.7 V as shown in figures 3(d)–(f). The microcracks seem to be induced by the internal stress which is caused by the formation of very hard Co-Mo alloy phase, while the nodules seem to be formed on the microcracks. The cathode current will

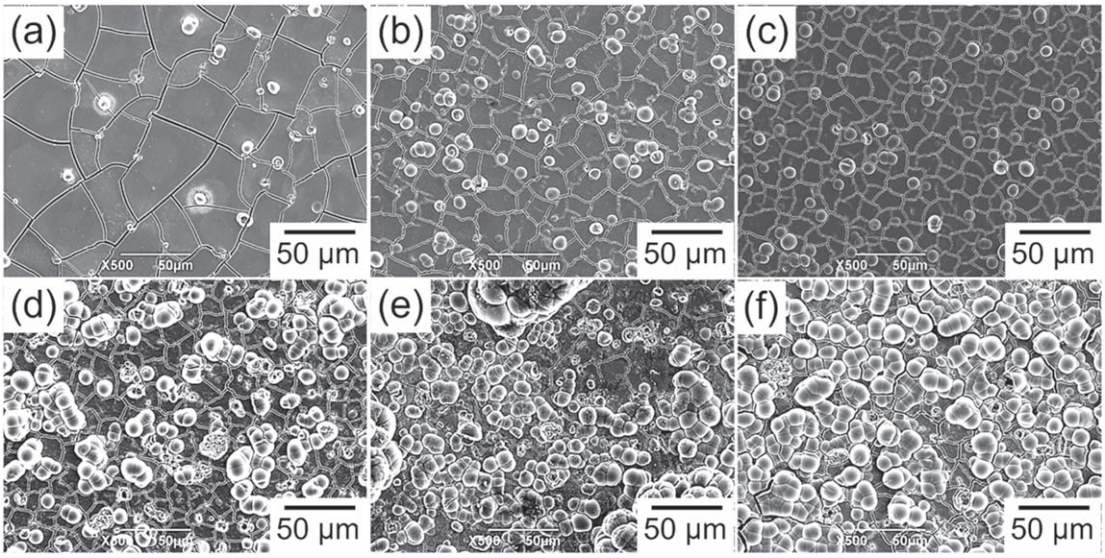

Figure 3. Effect of cathode potential on the SEM images of electrodeposited Co-Mo alloys ((a) $E = -1.2$ V, $X_{Mo} = 36\%$, (b) $E = -1.3$ V, $X_{Mo} = 38\%$, (c) $E = -1.4$ V, $X_{Mo} = 31\%$, (d) $E = -1.5$ V, $X_{Mo} = 39\%$, (e) $E = -1.6$ V, $X_{Mo} = 48\%$, (f) $E = -1.7$ V, $X_{Mo} = 53\%$).

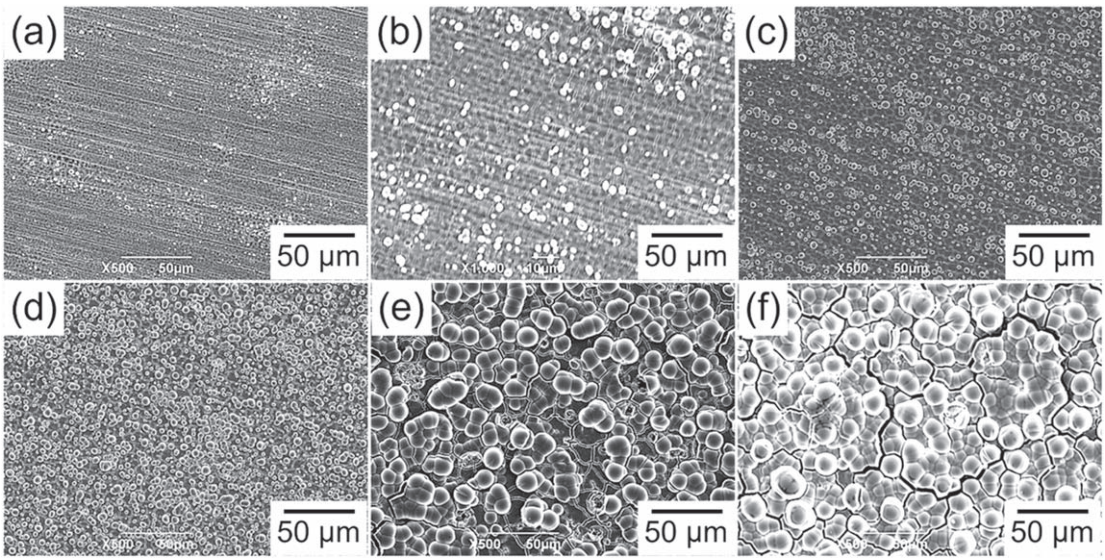

Figure 4. Effect of growth time on the SEM images of Co-53%Mo alloys electrodeposited at the cathode potential of −1.7 V ((a) $t = 5$ min, (b) $t = 10$ min, (c) $t = 15$ min, (d) $t = 30$ min, (e) $t = 60$ min, (f) $t = 90$ min).

be focused on the microcracks because the conductivity of copper substrate is greater than that of electrodeposited Co-Mo alloys. Consequently, the high current density on the microcracks will induce the three-dimensional nodule-like surface appearance.

Figure 4 shows the effect of growth time on the SEM images of Co-53%Mo alloys electrodeposited at the cathode potential of −1.7 versus The growth time was ranging from 5 min to 90 min. As shown in figures 4(a)–(d), in the growth time less than 30 min, small nodule nuclei with the diameter of approximately 3 μm are observed on the microcracks and the density of nuclei seems to increase with an increase in the growth time. On the contrary, as shown in figures 4(e) and (f), in the growth time more than 60 min, all nodule nuclei on the microcracks are grown up to the diameter of approximately 10 μm. This nodule nuclei formation process on the microcracks correspond well to that shown in figure 3. Pellicer *et al* reported that the effect of growth time on the surface morphology of Co-38%Mo alloys which were electrodeposited at the cathode potential of −1.3 V versus Ag/AgCl [24]. They revealed that the nodule nuclei size was enhanced with increasing the growth time and the film thickness. According to their report, the formation of microcracks on the electrodeposited Co-Mo alloys was inhibited by applying a reverse pulse plating method. In the present study, the samples were prepared by

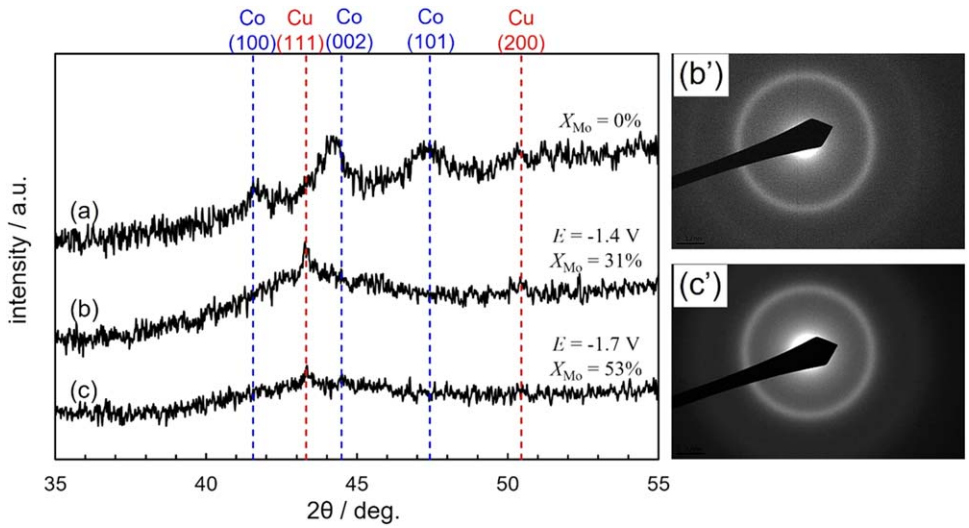

Figure 5. Effect of molybdenum content on the XRD profiles and ED patterns of electrodeposited Co-Mo alloys ((a) $X_{Mo} = 0\%$, (b) $E = -1.4$ V, $X_{Mo} = 31\%$, (c) $E = -1.7$ V, $X_{Mo} = 53\%$).

applying a potentiostatic electrodeposition technique. Hence, the microcracks and remarkable nodule nuclei seems to be observed in the samples which were electrodeposited in the growth time more than 60 min.

Figures 5(b) and (c) shows the effect of molybdenum content on the XRD profiles of Co–Mo alloys which were electrodeposited at the cathode potential of −1.4 V and −1.7 V versus Ag/AgCl. For comparison, the XRD profile of pure Co which was electrodeposited from a pure Co bath was also shown in figure 5(a). Here, the diffraction peaks, which are observed in the 2θ of 43.3° and 50.5°, are derived from Cu substrate. As shown in figure 5(a), broad peaks associated with hcp-Co (100), (002), and (101) were observed in the electrodeposited pure Co sample. However, except for the peaks from Cu substrate, no diffraction peaks were confirmed in the electrodeposited Co-Mo alloy samples as shown in figures 5(b) and (c). Hence, the electrodeposited Co-Mo alloys seems to be composed of an amorphous-like nanocrystalline phase. Ohgai *et al* revealed that the electrodeposited Ni-Mo alloys with more than 20% in X_{Mo} were composed of an amorphous-like nanocrystalline phase, while those with less than 20% in X_{Mo} consisted of polycrystalline phase [31, 32]. In the present study, the molybdenum content exceeded 30% as shown in figure 1(b). Hence, the nanocrystalline structure of electrodeposited Co-Mo alloys exhibited a similar tendency to that of electrodeposited Ni-Mo alloys.

Figures 5(b′) and (c′) shows the effect of molybdenum content on the electron diffraction patterns of Co-Mo alloys ((b′) $X_{Mo} = 31\%$ and (c′) $X_{Mo} = 53\%$). Concentric and vague diffraction patterns (halo-patterns) were observed as shown in the electron diffraction patterns. According to the radius of the broad ring pattern, the lattice spacing was estimated to be 0.228 nm which corresponds to that of hcp-Co (100). Hence, it was revealed that the electrodeposited Co-Mo alloys were composed of an amorphous-like nanocrystalline phase according to the electron diffraction patterns as well as the XRD profiles as shown in figures 5(b) and (c).

XPS spectra of the electrodeposited Co-Mo alloys ((a) $E = -1.4$ V, $X_{Mo} = 31\%$, (b) $E = -1.7$ V, $X_{Mo} = 53\%$) were shown in figure 6. The surface of each sample was etched by argon ions for a duration of 15 min. The binding energy that were derived from the metallic state of molybdenum corresponds to 231.0 eV (Mo°—$3d_{3/2}$) and 227.8 eV (Mo°—$3d_{5/2}$), while that of tetravalent molybdenum corresponds to 233.1 eV (Mo^{4+}—$3d_{3/2}$) and 229.8 eV (Mo^{4+}—$3d_{5/2}$). Hence, according to the XPS spectra (figure 6), molybdenum seems to exist as almost metallic state and a part of that also exists as an oxide state. Based on the above experimental results, molybdenum ions should form hydroxide in the vicinity of the cathode through a hydrolysis reaction during the electrodeposition process with a large over potential. Furthermore, the hydroxide could form metallic oxide and be included into the electrodeposited alloys via dehydration reaction.

3.3. Magnetization, micro-hardness, and heat-resistance performance of electrodeposited Co–Mo alloys

Figure 7 shows the effect of molybdenum content on the magnetic hysteresis loops of electrodeposited Co-Mo alloys ((a) $X_{Mo} = 0\%$, (b) $E = -1.4$ V, $X_{Mo} = 31\%$, (c) $E = -1.5$ V, $X_{Mo} = 39\%$, (d) $E = -1.6$ V, $X_{Mo} = 48\%$, (e) $E = -1.7$ V, $X_{Mo} = 53\%$). An external magnetic field was applied to in-plane direction to the electrodeposited alloy films. Figure 8(a) shows the effect of molybdenum content on the coercivity of electrodeposited Co-Mo alloys. In the figure, the coercivity value (118 Oe) of commercially available pure cobalt foil (purity: 99.9%) was also plotted as $X_{Mo} = 0\%$. The coercivity of electrodeposited Co-Mo alloys decreased to

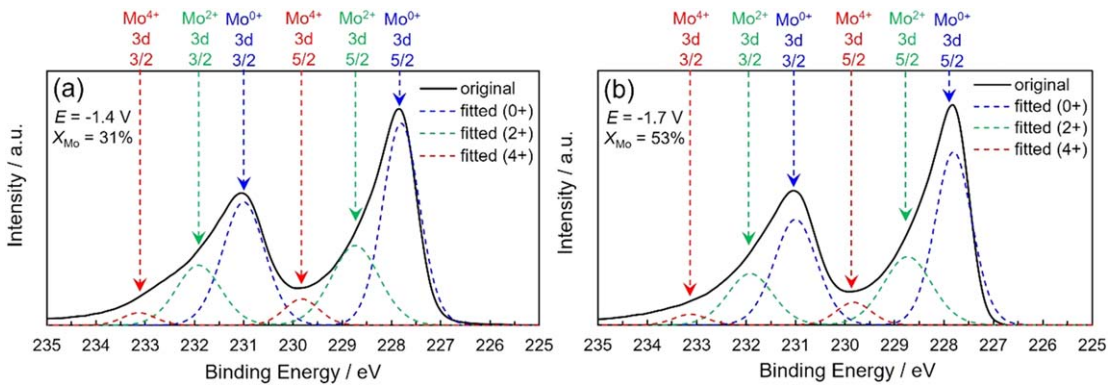

Figure 6. Effect of molybdenum content on the XPS spectra of electrodeposited Co-Mo alloys ((a) $E = -1.4$ V, $X_{Mo} = 31\%$, (b) $E = -1.7$ V, $X_{Mo} = 53\%$). The black solid lines correspond to the original plots while the blue, green and red dashed lines correspond to the fitted plots for Mo^{0+}, Mo^{2+} and Mo^{4+} spectra, respectively.

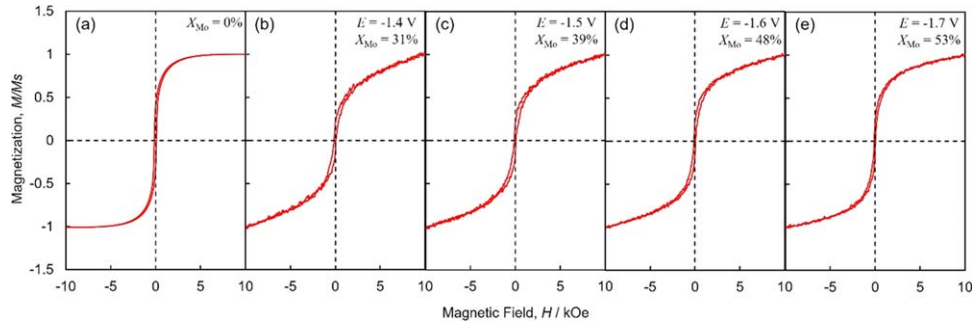

Figure 7. Effect of molybdenum content on the magnetic hysteresis loops of Co-Mo alloys ((a) $X_{Mo} = 0\%$, (b) $E = -1.4$ V, $X_{Mo} = 31\%$, (c) $E = -1.5$ V, $X_{Mo} = 39\%$, (d) $E = -1.6$ V, $X_{Mo} = 48\%$, (e) $E = -1.7$ V, $X_{Mo} = 53\%$).

72 Oe with an increase in X_{Mo} up to ca. 53%. Gómez *et al* also reported that the coercivity of electrodeposited pure Co was around 140 Oe while that of Co-Mo alloys, which were electrodeposited from an aqueous solution containing citric acid, decreased down to a quite small value [33]. Herzer *et al* reported that the coercivity, H_c of ferromagnetic materials strongly depended on the average crystal grain diameter, D [34]. According to their report, H_c is in proportion to D^{-1} in the ferromagnetic materials with a multi-domain structure, while that is proportional to D^6 in those with a superparamagnetic structure. As shown in figure 5, the electrodeposited Co-Mo alloys have an amorphous-like nanocrystalline structure. Hence, in the present study, the coercivity of electrodeposited Co-Mo alloys decreased due to the reduction in the average crystal grain diameter, D with an increase in the molybdenum content, X_{Mo}. Figure 8(b) shows the effect of molybdenum content on the microhardness of electrodeposited Co-Mo alloys. It has been reported that the hardness of electrodeposited pure cobalt was approximately 130 kgf mm^{-2} (HV) [35]. In this study, the microhardness of commercially available cobalt foil was determined to be 291.1 kgf mm^{-2} ($HV_{0.05}$). As shown in figure 8(b), the microhardness of electrodeposited Co-Mo alloys increased up to 845 kgf mm^{-2} ($HV_{0.1}$) with an increase in X_{Mo} up to 53%. According to the mechanism of solid solution strengthening of metallic materials, the density of lattice defects, such as dislocations and grain boundaries, increases with an increase in the concentration of solute atoms. Furthermore, the average crystal grain size will decrease with an increase in the density of lattice defects. Hence, in this study, the synergistic effect of solid solution strengthening and crystal grain refinement seems to have contributed to improving the microhardness of electrodeposited Co-Mo alloys.

Figure 9 shows the effect of annealing temperature on the XRD profiles of Co-53%Mo alloys which were electrodeposited at the cathode potential of −1.7 versus As-deposited sample (a) was annealed at 100 °C (b), 300 °C (c), 500 °C (d), 700 °C (e), and 900 °C (f). The annealing was conducted for 1 h under argon gas atmosphere.

According to the binary alloy phase diagram of Co-Mo system [36], intermetallic compounds such as Co_3Mo, Co_7Mo_6 and Co_2Mo_3 will be appeared as the stable phases in Co-53%Mo alloy. However, in the present study, in the temperature range less than 700 °C, the diffraction peaks which are derived from Co alloy phases were not observed as shown in figures 9(b)–(d). While, in the temperature range from 700 °C to 900 °C, the diffraction peak which is derived from $CoMoO_4$ (330) was clearly observed at 2θ of around 43.2° as shown in

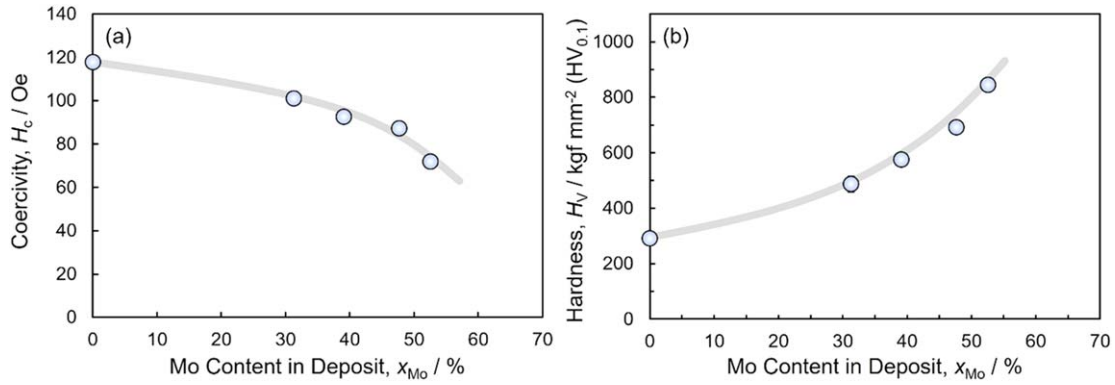

Figure 8. Effect of molybdenum content on the coercivity (a) and microhardness (b) of Co-Mo alloys.

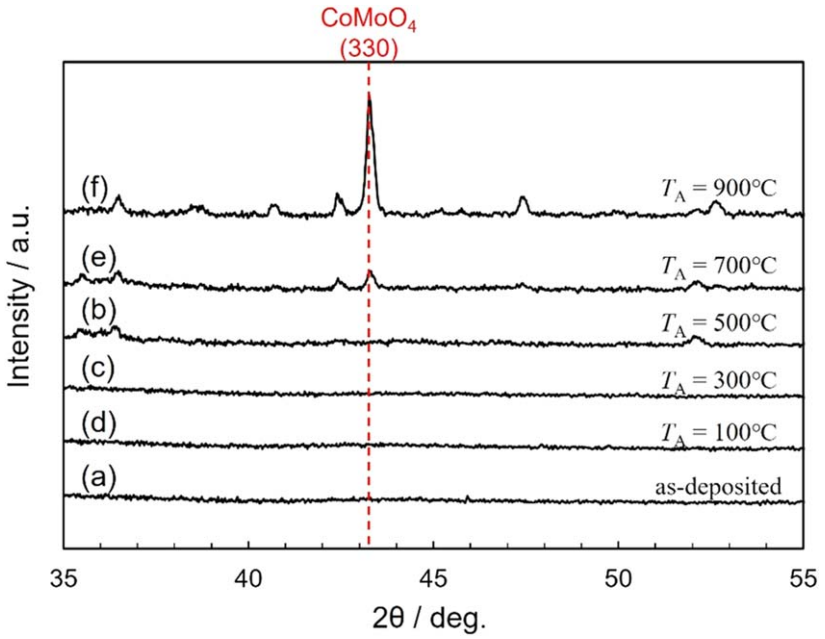

Figure 9. Effect of annealing temperature on the XRD profiles of Co-53%Mo alloys electrodeposited at the cathode potential of −1.7 V ((a) as-deposited, (b) T_A = 100 °C, (c) T_A = 300 °C, (d) T_A = 500 °C, (e) T_A = 700 °C, (f) T_A = 900 °C). Each sample was annealed for 1 h under argon gas atmosphere.

figures 9(e) and (f). As shown in figures 5 and 6, as-deposited sample was composed of an amorphous-like nanocrystalline structure with a metallic Co-Mo alloy phase and a molybdenum oxide phase such as MoO and MoO_2. Hence, this $CoMoO_4$ phase seems to be formed by alloying reaction between the metallic Co-Mo phase and the molybdenum oxide phase during the high temperature annealing process more than 700 °C. The molybdenum oxide phase could be involved in the electrodeposit during the above mentioned '*induced co-deposition*' process.

4. Conclusion

Co-Mo alloys were synthesized from an aqueous solution using a potentiostatic electrodeposition technique. Molybdenum content in the alloy films was controlled up to 53% by shifting the electrode potential down to −1.7 V versus Ag/AgCl. Amorphous-like nanocrystalline structure was observed in the electrodeposited Co-Mo alloys. Coercivity of the electrodeposited Co-Mo alloys decreased down to 72 Oe with an increase in X_{Mo} up to ca. 53%. Microhardness increased up to 845 kgf mm^{-2} with an increase in X_{Mo} up to 53%. It was concluded that the synergistic effect of solid solution strengthening and crystal grain refinement strengthening contributed to improve the microhardness and heat-resistance performance of electrodeposited Co-Mo alloys.

Acknowledgments

The authors thank Japan Society for the Promotion of Science (JSPS: 18H01754 and 20J21925) for the financial support.

Data availability statement

The data that support the findings of this study are available upon reasonable request from the authors.

Declarations

Competing interests

The authors declare that they have no competing interests.

Authors' contributions

TM, RS and MH carried out experiments, analyzed data, and wrote manuscript. TO designed the study, supervised the project, and analyzed data. All authors read and approved the final manuscript.

ORCID iDs

Takeshi Ohgai https://orcid.org/0000-0001-6872-7888

References

[1] Lausmann G A 1996 Electrolytically deposited hardchrome *Surf. Coat. Technol.* **86–87** 814–20
[2] Zeng Z, Wang L, Chen L and Zhang J 2006 The correlation between the hardness and tribological behaviour of electroplated chromium coatings sliding against ceramic and steel counterparts *Surf. Coat. Technol.* **201** 2282–8
[3] Giovanardi R and Orlando G 2011 Chromium electrodeposition from Cr(III) aqueous solutions *Surf. Coat. Technol.* **205** 3947–55
[4] Danilov F I, Protsenko V S, Gordiienko V O, Kwon S C, Lee J Y and Kim M 2011 Nanocrystalline hard chromium electrodeposition from trivalent chromium bath containing carbamide and formic acid: structure, composition, electrochemical corrosion behavior, hardness and wear characteristics of deposits *Appl. Surf. Sci.* **257** 8048–53
[5] Protsenko V S, Danilov F I, Gordiienko V O, Kwon S C, Kim M and Lee J Y 2011 Electrodeposition of hard nanocrystalline chrome from aqueous sulfate trivalent chromium bath *Thin Solid Films* **520** 380–3
[6] Ohgai T, Tanaka Y and Fujimaru T 2012 Soft magnetic properties of Ni–Cr and Co–Cr alloy thin films electrodeposited from aqueous solutions containing trivalent chromium ions and glycine *J. Appl. Electrochem.* **42** 893–9
[7] Weston D P, Shipway P H, Harris S J and Cheng M K 2009 Friction and sliding wear behaviour of electrodeposited cobalt and cobalt–tungsten alloy coatings for replacement of electrodeposited chromium *Wear* **267** 934–43
[8] Ohgai T, Fujimaru T and Tanaka Y 2014 Isotropic magnetization response of electrodeposited nanocrystalline Ni–W alloy nanowire arrays *J. Appl. Electrochem.* **44** 301–7
[9] Brenner A 1963 *Electrodeposition of Alloys* (New York: Academic)
[10] Gomez E, Pellicer E, Duch M, Esteve J and Valles E 2006 Molybdenum alloy electrodeposits for magnetic actuation *Electrochim. Acta* **51** 3214–22
[11] Abdel Hamid Z, Abdel Aal A, Shaaban A and Hassan H B 2009 Electrodeposition of CoMoP thin film as diffusion barrier layer for ULSI applications *Surf. Coat. Technol.* **203** 3692–700
[12] Tanase S I, Pinzaru Tanase D, Dobromir M and Georgescu V 2011 Morphology, magnetic, magnetoresistance and optical properties of Co–Ni–Mo alloys thin films *Appl. Surf. Sci.* **257** 10903–9
[13] Messaoudi Y, Fenineche N, Guittoum A, Azizi A, Schmerber G and Dinia A 2013 A study on electrodeposited Co–Mo alloys thin films *J. Mater. Sci., Mater. Electron.* **24** 2962–9
[14] Zhou Q F, Lu L Y, Yu L N, Xu X G and Jiang Y 2013 Multifunctional Co–Mo films fabricated by electrochemical deposition *Electrochim. Acta* **106** 258–63
[15] Krawiec H, Vignal V, Latkiewicz M and Herbst F 2018 Structure and corrosion behaviour of electrodeposited Co-Mo/TiO_2 nano-composite coatings *Appl. Surf. Sci.* **427** 1124–34
[16] Costovici S, Manea A C, Visan T and Anicai L 2016 Investigation of Ni—Mo and Co—Mo alloys electrodeposition involving choline chloride based ionic liquids *Electrochim. Acta* **207** 97–111
[17] Mukhamedova G Y, Ved M, Sakhnenko N and Nenastina T 2018 Electrodeposition and properties of binary and ternary cobalt alloys with molybdenum and tungsten *Appl. Surf. Sci.* **445** 298–307
[18] Wang C and Podlaha E J 2020 Electrodeposited Co–Mo–P–TiO_2 composites electrocatalysts for the hydrogen evolution reaction *J. Electrochem. Soc.* **167** 132502
[19] Casciano P N S, Benevides R L, Santana R A C, Correia A N and Lima-Neto P 2017 Factorial design in the electrodeposition of Co-Mo coatings and their evaluations for hydrogen evolution reaction *J. Alloy. Compd.* **723** 164–71

[20] Yar-Mukhamedova G, Ved M, Sakhnenko N and Koziar M 2017 Ternary cobalt-molybdenum-zirconium coatings for alternative energies *Appl. Surf. Sci.* **421** 68–76
[21] Kuznetsov V V, Gamburg Y D, Zhulikov V V, Krutskikh V M, Filatova E A, Trigub A L and Belyakova O A 2020 Electrodeposited NiMo, CoMo, ReNi, and electroless NiReP alloys as cathode materials for hydrogen evolution reaction *Electrochim. Acta* **354** 136610
[22] Laszczynska A and Szczygieł I 2020 Electrocatalytic activity for the hydrogen evolution of the electrodeposited Co–Ni–Mo, Co–Ni and Co–Mo alloy coatings *Int. J. Hydrog. Energy* **45** 508–20
[23] Santos H L S, Corradini P G, Medina M and Mascaro L H 2020 Effect of copper addition on cobalt-molybdenum electrodeposited coatings for the hydrogen evolution reaction in alkaline medium *Int. J. Hydrog. Energy* **45** 33586–97
[24] Pellicer E, Gómez E and Vallés E 2006 Use of the reverse pulse plating method to improve the properties of cobalt–molybdenum electrodeposits *Surf. Coat. Technol.* **201** 2351–7
[25] Krawiec H, Vignal V, Krystianiak A, Gaillard Y and Zimowski S 2019 Mechanical properties and corrosion behaviour after scratch and tribological tests of electrodeposited Co–Mo/TiO_2 nano-composite coatings *Appl. Surf. Sci.* **475** 162–74
[26] Neetzel C, Ohgai T, Yanai T, Nakano M and Fukunaga H 2017 Uniaxial magnetization performance of textured Fe nanowire arrays electrodeposited by a pulsed potential deposition technique *Nanoscale Res. Lett.* **12** 598
[27] Saeki R and Ohgai T 2018 Determination of activation overpotential during the nucleation of hcp-cobalt nanowires synthesized by potentio-static electrochemical reduction *Materials* **11** 2355
[28] Gomez E, Pellicer E and Valles E 2005 An approach to the first stages of cobalt–nickel–molybdenum electrodeposition in sulphate–citrate medium *J. Electroanal. Chem.* **580** 222–30
[29] Saeki R and Ohgai T 2020 Perpendicular magnetization performance of hcp-cobalt nanocylinder array films electrodeposited from an aqueous solution containing cobalt (II)–citrate complexes *J. Mater. Res. Technol.* **9** 8029–40
[30] Gomez E, Pellicer E and Valles E 2003 Influence of the bath composition and the pH on the induced cobalt-molybdenum electrodeposition *J. Electroanal. Chem.* **556** 137–45
[31] Ohgai T, Tanaka Y and Washio R 2013 Nanocrystalline structure and soft magnetic properties of nickel–molybdenum alloy thin films electrodeposited from acidic and alkaline aqueous solutions *J. Solid State Electrochem.* **17** 743–50
[32] Ohgai T, Washio R and Tanaka Y 2012 Anisotropic magnetization behavior of electrodeposited nanocrystalline Ni-Mo alloy thin films and nanowires array *J. Electrochem. Soc.* **159** H800–4
[33] Gomez E, Pellicer E and Valles E 2001 Electrodeposited cobalt-molybdenum magnetic materials *J. Electroanal. Chem.* **517** 109–16
[34] Herzer G 1990 Grain size dependence of coercivity and permeability in nanocrystalline ferromagnets *IEEE Trans. Magn.* **26** 1397–402
[35] Hagiwara H, Kaneko Y and Uchida M 2020 Fabrication and enhanced vickers hardness of electrodeposited CoCu alloy film with high composition gradient *Mater. Trans.* **61** 801–4
[36] Okamoto H 2007 Co-Mo (Cobalt-Molybdenum) *J. Phase Equilib. Diffus.* **28** 300